HTML ABSTRACT + LINKS

JOURNAL OF APPLIED PHYSICS **97**, 023527 (2005)

In situ real-time spectroscopic ellipsometry study of HfO_2 thin films grown by using the pulsed-source metal-organic chemical-vapor deposition

Yangdong Zheng
Quantum Nanoelectronics Research Center, Tokyo Institute of Technology, 2-12-1 O-okayama, Meguro-Ku Tokyo 152-8552, Japan

Hiroshi Mizuta
Quantum Nanoelectronics Research Center and Department of Physical Electronics, Tokyo Institute of Technology, 2-12-1 O-okayama, Meguro-Ku Tokyo 152-8552, Japan

Yoshishige Tsuchiya, Masato Endo, Daisuke Sato, and Shunri Oda[a)]
Quantum Nanoelectronics Research Center, Tokyo Institute of Technology, 2-12-1 O-okayama, Meguro-Ku Tokyo 152-8552, Japan

(Received 21 June 2004; accepted 13 October 2004; published online 27 December 2004)

The HfO_2 thin-film growth process is investigated by using *in situ* real-time spectroscopic ellipsometry (SE) technique combined with the first-principles molecular-orbital (MO) calculations of the electronic states. The HfO_2 films are grown on the silicon substrate by using the pulsed-source metal-organic chemical-vapor deposition method. Particular attention is paid to the formation of an interfacial layer at the early stage of the growth process by monitoring energy-dependent dielectric constants of the film. The energy dependence of the electronic polarizabilities and dielectric constants is calculated for the amorphous HfO_2, SiO_2, and $HfSiO_4$ films based on the electronic states and density of states obtained using the discrete-variational $X\alpha$ MO method with the unit cluster model. The measured SE spectra show that the average dielectric constants of the film vary gradually from those for SiO_2 to those for HfO_2 when the number of deposition cycles increases. By comparing the varied dielectric constants during the film growth with the calculated results, we find that the HfO_2 film growth process can be divided into two stages with different growth mechanisms: SiO_2 and $Hf_xSi_yO_z$ layers are grown at the first stage, which are regarded as the interfacial layers, and the HfO_2 layer formation becomes predominant at the second stage. © *2005 American Institute of Physics*. [DOI: 10.1063/1.1827912]

I. INTRODUCTION

Present microelectronics industry depends on continuous miniaturization of the integrated circuit components, especially metal-oxide-silicon field-effect transistors (MOSFETs). As the MOSFETs scale down to below 100 nm, the alternative gate dielectrics with a dielectric constant k higher than that of SiO_2, hence with a larger capacitance equivalent thickness, are desired since the issue of gate leakage current due to direct tunneling through the conventional gate insulator SiO_2 has become increasingly serious. The high dielectric constant (high-k) oxide films with the large band gap, the low defect density, and the thermodynamical stability in contact with silicon are attracting great interest as a replacement to the SiO_2 films,[1–3] and among many potential materials, HfO_2 has particularly been highlighted recently.[4–7]

However, most vapor phase grown HfO_2 thin films appear to contain interfacial layers (ILs) at the film-substrate interface. The formation of the IL during the film growth is one of the most crucial issues and is more or less inevitable due to the chemical reaction processes and $Si \leftrightarrow O$ interdiffusions across the growth surface. This reduces the overall capacitance, because the IL may be composed of the silicate layer, which shows the dielectric constant smaller than that of HfO_2.[8] In addition, the presence of the IL affects the electrical characteristics, such as the channel mobility or the threshold voltage for the MOSFETs, significantly due to the interface trapped charge and the oxide fixed charge.

The purpose of this paper is to investigate the growth process of the HfO_2 thin film by using the *in situ* real-time spectroscopic ellipsometry (SE) technique. In particular, the mechanism of the interfacial layer formation at the early stage of the growth is discussed by analyzing the change in the dielectric constant dispersions incident to the film growth. In order to extract the dielectric constant dispersions from the measured SE spectra, we need information about the optical properties of the materials produced in the HfO_2 film growth, e.g., $Hf_xSi_yO_z$. Unfortunately, neither the experimental nor the theoretical results reported to date are sufficient to do this for the HfO_2 or $HfSiO_4$ amorphous materials, and therefore, we perform the theoretical analysis based on the discrete-variational $X\alpha$ (DV-$X\alpha$) first-principles molecular-orbital (MO) calculations. Based on these experimental and theoretical results, we finally propose an atomistic model for the HfO_2 film growth process.

[a)]Author to whom correspondence should be addressed; electronic mail: soda@pe.titech.ac.jp

 © 2005 American Institute of Physics

Downloaded 21 Jul 2008 to 152.78.61.227. Redistribution subject to AIP license or copyright; see http://jap.aip.org/jap/copyright.jsp

II. REAL-TIME SPECTROSCOPIC ELLIPSOMETRY MEASUREMENTS FOR HfO_2 THIN FILMS

In our experiments, HfO_2 thin films were deposited by the pulsed-source metal-organic chemical-vapor deposition (MOCVD) method,[9] which can be regarded as an atomic layer deposition technique to realize the layer-by-layer deposition in the CVD. A spectroscopic phase modulated ellipsometer (UVISEL™: Jovin-Yvon, Inc.[10]) was introduced in the CVD chamber for the spectroscopic ellipsometry observation during the film growth. $Hf[N(CH_3)_2]_4$ and O_2 were used as the precursor and oxidant with the duration of 3 and 40 s, respectively. Ar purge was used between each chemical pulse for 20 s. Consequently, the total process time for each cycle was 83 s, and we grew the film with a thickness of about 6 nm in 35 cycles. The *p*-type Si(100) substrate was used, and the substrate temperature was maintained at 300 °C during the deposition so that the grown HfO_2 film would be in the amorphous phase. This is because a lower leakage current is expected for the films grown in the amorphous phase than those grown in the crystalline phase. The native oxide on the Si wafer surface was removed with HF dipping immediately prior to the film growth. The equivalent oxide thickness (EOT) and the leakage currents via the grown HfO_2 dielectric films were obtained from the $C-V$ and $I-V$ measurements. The physical thickness of the HfO_2 film was extracted from the cross-section transmission electron microscopy (TEM) images. The spatial distributions of Hf, O, and Si in the films were also evaluated by using energy dispersive x-ray spectroscopy (EDX) analysis.

The *in situ* spectroscopic ellipsometry has widely been used to study thin-film growth processes because it facilitates monitoring the change in the average composition of the entire film by measuring the dielectric functions.[11,12] We conducted the spectroscopic ellipsometry measurements at various stages of the layer-by-layer deposition process to track the development of the film *in situ* and at real time. Further details about the experimental setup and the UV-visible ellipsometer can be found elsewhere.[13,14]

Optical properties of any medium can be described by the complex index of refraction, $N=n+ik$, or the complex dielectric function, $\varepsilon=\varepsilon_r+i\varepsilon_i$. ε and N are related to each other by $\varepsilon=N^2$, and so the real and imaginary parts of ε can also be determined from the refractive index n and the extinction coefficient k, $\varepsilon_r=n^2-k^2$ and $\varepsilon_i=2nk$. In principle, the ellipsometry measures Ψ and Δ, which denote the changes in the amplitude and phase of polarization between the incident and reflected waves,

$$\Psi = \tan^{-1}\left(\frac{|r_p|}{|r_s|}\right), \tag{1}$$

$$\Delta = \delta_p - \delta_s, \tag{2}$$

where r and δ give the amplitude ratio and the phase shift between the electric vector of the reflected waves and incident waves. The subscripts p and s refer to the plane-wave electric-field components, parallel and perpendicular to the plane of incidence.[15]

In this study, we used a one-layer model to calculate the average dielectric function of the film from (Ψ,Δ) measured just before (e.g., the Si substrate) and after the film deposition. First, making use of Snell's law and Fresnel's law, the dielectric function of the substrate ε_{sub} can be derived as follows:

$$\varepsilon_{\text{sub}} = \varepsilon_{\text{sub}} + i\varepsilon_{\text{sub}} = \varepsilon_0 \sin^2 \phi_0\left[1+\left(\frac{1-\rho}{1+\rho}\right)^2 \tan^2 \phi_0\right], \tag{3}$$

where ε_0 and ϕ_0 represent the vacuum permittivity and an angle of incidence (71° in our experimental setup). The ratio ρ is given by

$$\rho = \frac{r_{p_\text{sub}}}{r_{s_\text{sub}}} = \tan(\Psi_{\text{sub}})\exp(i\Delta_{\text{sub}}), \tag{4}$$

where r is the Fresnel coefficient for reflection between the ambient and the substrate (we hereafter denote this as ambient substrate), which can be represented by ϕ_0 and the complex index of refraction of the substrate N_{sub}.[16] Next, we get the dielectric function of the film $\varepsilon_{\text{Layer}}$ using the following equations:

$$R_p = \frac{r_{01p} + r_{12p}e^{-2i\delta}}{1 + r_{01p}r_{12p}e^{-2i\delta}} = |R_p|e^{i\delta_{Rp}},$$
$$R_s = \frac{r_{01s} + r_{12s}e^{-2i\delta}}{1 + r_{01s}r_{12s}e^{-2i\delta}} = |R_s|e^{i\delta_{Rs}}, \tag{5}$$

$$\delta = \frac{2\pi d_1 n_1 \cos \phi_1}{\lambda}, \tag{6}$$

$$\frac{R_p}{R_s} = \tan(\Psi_{\text{Layer}})\exp(i\Delta_{\text{Layer}}), \tag{7}$$

where the subscripts 01 and 12 denote ambient film and film substrate, respectively. In Eq. (5), δ represents the phase shift of light in the film, d_1 and n_1 are the thickness and the refractive index of the film, and φ_1 and λ are the angle of incidence and the wavelength of the light.

By substituting Eqs. (5) and (6) with Eq. (7), we obtain a complex number equation, which can be converted into two real number equations. On the other hand, when the dielectric oxide film is a transparent material, the imaginary part of $\varepsilon_{\text{Layer}}$ ($\varepsilon_{\text{Layer_im}}$) is zero. Therefore, two unknown parameters, the real part of $\varepsilon_{\text{Layer}}$ ($\varepsilon_{\text{Layer_}r}$) and the film thickness $d_{\text{Layer}}(d_1)$, can be obtained from Eqs. (5)–(7) in principle with the experimental results. In our study, by setting an initial guess obtained from the results of the fitting or other evaluation methods, the numerical calculations were performed to find a set of $(\varepsilon_{\text{Layer_}r}, d_{\text{Layer}})$ that reproduce the experimental results the best. The unbiased estimator of the mean-square deviation is obtained for individual energy points of the measured spectrum as follows:

$$\text{Err} = \sqrt{(\Psi_{\text{cal}} - \Psi_{\text{exp}})^2 + (\Delta_{\text{cal}} - \Delta_{\text{exp}})^2}, \tag{8}$$

where the subscripts exp and cal are the experimental and calculated values.

Downloaded 21 Jul 2008 to 152.78.61.227. Redistribution subject to AIP license or copyright; see http://jap.aip.org/jap/copyright.jsp

III. THEORETICAL ANALYSIS OF DIELECTRIC CONSTANTS FOR THE HfO_2, SiO_2, AND $HfSiO_4$ CLUSTERS

The optical constants, $N(E)=n(E)+ik(E)$ or $\varepsilon(E)=\varepsilon_r(E)+i\varepsilon_i(E)$, are defined as a function of the photon energy, $E=\hbar\omega=hc/\lambda$, and these are called optical dispersion relations. Here ω and λ represent the photon frequency and wavelength, respectively, and c is the speed of light. Because the photon energy used for the ellipsometry is in the ultraviolet-to-visible region, only the electronic dielectric dispersions are discussed in this study.

Generally, a procedure for computing the electronic dielectric constants of the amorphous materials can be described in the following three steps: (1) defining a suitable unit cluster from the amorphous structures, whose electronic states are expected to be similar to those of the amorphous materials, (2) calculating the electronic states of the cluster, and (3) calculating the energy-dependent electronic dielectric constants of the cluster from the electronic states. In this study, steps (1) and (2) were carried out by using the DV-$X\alpha$ first-principles MO methods. The theoretical details of the DV-$X\alpha$ method are summarized in the Appendix, and so only step (3) is explained in this section.

Based on the first-order time-dependent perturbation thoery,[17,18] the polarizability and the photon transition probability can be obtained from the calculated electronic states. For the isotropic medium, e.g., amorphous materials, the optical polarizability is given by

$$\alpha(\omega)=\frac{2e^2}{2\hbar}\sum_{n,n'}\left(\frac{\omega_{nn'}}{\omega_{nn'}{}^2-\omega^2}|\langle n|\boldsymbol{r}_{nn'}|n'\rangle|^2\right)$$
$$=\frac{e^2}{m}\sum_{n,n'}\frac{f_{nn'}}{\omega_{nn'}{}^2-\omega^2}$$
$$=\frac{e^2}{m}\int\int\left(\frac{f_{nn'}}{\omega_{nn'}{}^2-\omega^2}DS_nDS_{n'}\right)dE_ndE_{n'}, \qquad (9)$$

where e and m are the electron charge and mass, ω is the photon frequency, $\omega=E/\hbar$, and $\omega_{nn'}$ is the transition frequency related to MOs energy, $\omega_{nn'}=(E_n-E_{n'})/\hbar$. $|n\rangle$ and $|n'\rangle$ denote the wave functions of the unoccupied MOs and the occupied MOs, and $\boldsymbol{r}_{nn'}$ is the position operator. DS_n and $DS_{n'}$ represent the density of state (DOS) of the unoccupied MOs and the occupied MOs, respectively. The optical oscillator strength that means the number of optical oscillators is given by

$$f_{n'n}=\frac{2m\omega_{nn'}}{3\hbar}|\langle n|\boldsymbol{r}_{nn'}|n'\rangle|^2. \qquad (10)$$

Since the excited state $|n\rangle$ has an finite lifetime, the photon relaxation process must be considered,[16,17] the relaxation coefficient $\gamma_{nn'}$ is added in Eq. (8) as follows:

$$\alpha(\omega)=\frac{e^2}{m}\int\int\left\{\frac{f_{nn'}(\omega_{nn'}{}^2-\omega^2)^2}{(\omega_{nn'}{}^2-\omega^2)^2+\gamma_{nn'}^2\omega^2}DS_nDS_{n'}\right\}\times dE_ndE_{n'}. \qquad (11)$$

In this study, we used Eq. (11) to compute the electronic polarizabilities.

For calculating the real parts of ε from the polarizability above, we used the following Lorentz–Lorenz formula:

$$\frac{\varepsilon-1}{\varepsilon+2}=\frac{N_m\alpha}{3\varepsilon_0}, \qquad (12)$$

where ε_0 and N_m are the vacuum permittivity and the number of clusters per unit volume, respectively.

On the other hand, the probability for the photon transition from the unoccupied MOs to the occupied MOs per unit time is given by

$$w(\omega)=\frac{3\pi e^2N_m}{2m\varepsilon_0}\sum_{n,n'}\{f_{nn'}\delta(\omega-\omega_{nn'})\}$$
$$=\frac{3\pi e^2N_m}{2m\varepsilon_0}\int\int\{f_{nn'}\delta(\omega-\omega_{nn'})DS_nDS_{n'}\}dE_ndE_{n'}, \qquad (13)$$

where the parameters in the equation are the same as those in Eqs. (9) and (12).

By using the relationship between w and the absorption coefficient Γ, $\Gamma(\omega)=w(\omega)n/c$, as well as that between the k and Γ, $\Gamma(\omega)=2\omega k(\omega)/c$,[18] the extinction coefficient k can be derived as follows:

$$k(w)=\frac{3\pi e^2nN_m}{4m\varepsilon_0\omega}\sum_{n,n'}\{f_{nn'}\delta(\omega-\omega_{nn'})\}$$
$$=\frac{3\pi e^2nN_m}{4m\varepsilon_0\omega}\int\int\{f_{nn'}\delta(\omega-\omega_{nn'})DS_nDS_{n'}\}dE_ndE_{n'}, \qquad (14)$$

where n is the refractive index of the medium.

In this work we first calculated the electronic states for the HfO_2, SiO_2, and $HfSiO_4$ cluster models shown in Fig. 8 by using the DV-$X\alpha$ methods (see Appendix). The calculated DOSs are shown in Fig. 1 for the three clusters: DOSs (right-hand side) and the orbital resolved partial DOSs (PDOSs) (left-hand side) for the occupied and unoccupied MOs near the band gap that correspond to the valence band and the conduction band, respectively. From the calculated DOSs, we derived the band gaps between the highest occupied molecular orbital and the lowest unoccupied molecular orbital (LUMO). As seen in Fig. 1, the band gaps of HfO_2, SiO_2, and $HfSiO_4$ clusters are approximately 4.9, 10.5, and 4.6 eV. These results are qualitatively consistent with the band-gap values taken from the latest literatures.[19] There have been several earlier reports on the electronic states for SiO_2 (polymorphic forms) and monoclinic HfO_2 through the first-principles pseudopotential calculations. For example, the band gaps of 5.59 (Ref. 20) and 5.8 eV (Ref. 21) were reported for the a-quartz SiO_2, and those of 3.6 (Ref. 22) and

Downloaded 21 Jul 2008 to 152.78.61.227. Redistribution subject to AIP license or copyright; see http://jap.aip.org/jap/copyright.jsp

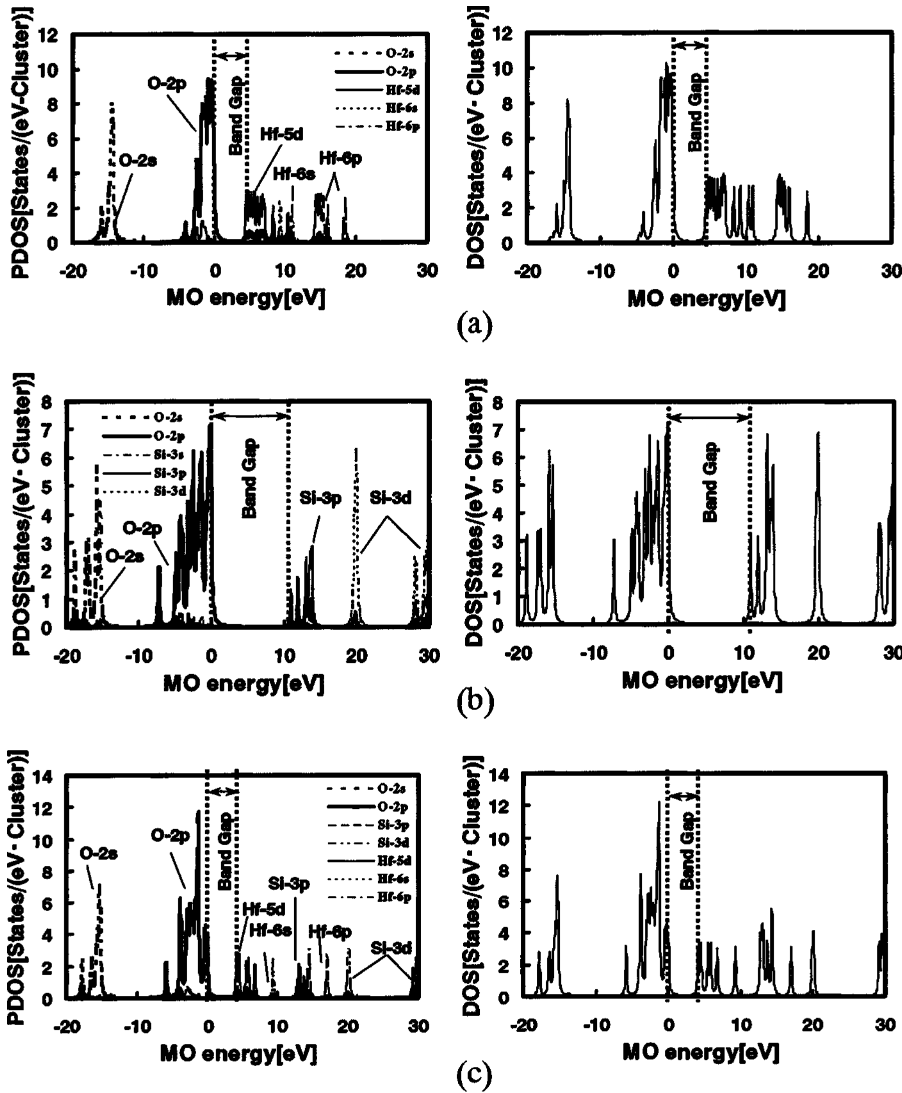

FIG. 1. Density of states (DOS) and orbital resolved partial DOS (PDOS) of the occupied and unoccupied MOs near the band gap for the HfO_2, SiO_2, and $HfSiO_4$ clusters. PDOS (left) and DOS (right) for (a) the HfO_2 cluster and (b) the SiO_2 cluster.

4.12 eV (Ref. 23) for the monoclinic HfO_2. These band-gap values are still much smaller than the experimental value of 8.9 eV for SiO_2 and 5.68 eV for HfO_2. It is intriguing that our present results of 10.5 eV for SiO_2 and 4.9 eV for HfO_2 are closer to the experimental values. This may indicate that our cluster model extracted from the amorphous random-network structures works well despite its simplicity.

It should be noted that the band gaps for HfO_2 and $HfSiO_4$ are almost the same because these are basically determined by the weak interactions between Hf-5*d* and the other kinds of atomic orbitals (Hf-5*d* is a nonbonding orbital). The DOS distributions also show that the occupied MOs predominantly consist of the O-2*s* and O-2*p* orbitals while the unoccupied MOs consist of Hf-5*d*, Hf-6*s*, and Hf -6*p* orbitals for HfO_2, and Si-3*p*, Si-3*d*, and Si-3*s* orbitals for SiO_2. In contrast, the DOS near the top or bottom of the band gap is larger than that at other energies. Moreover, the results indicate that the band gap for the $Hf_xSi_yO_z$ cluster is similar to that for HfO_2 mainly because the Hf-5*d* orbital forms the LUMO state. Furthermore, the unoccupied MOs for $Hf_xSi_yO_z$ are composed of the Hf outermost atomic orbitals, 5*d*, 6*s*, and 6*p*, as well as the Si outermost atomic orbital, 3*p*, 3*d*, and 3*s*. A trend is seen that the greater the compositional ratio of the Hf element is $(x>y)$, the higher the Hf outermost orbital densities are. Inversely, the greater the concentration of Si element is $(x<y)$, the higher the Si outermost orbital densities are. These facts are useful for predicting the optical properties of the $Hf_xSi_yO_z$.

Based on these electronic states, we then computed the polarizability and dielectric constants of the HfO_2, SiO_2, and $HfSiO_4$ amorphous films by using the obtained band gaps and DOS distributions with Eqs. (10)–(12). The parameters used in the calculation are summarized in Table I. The oscil-

TABLE I. Parameters used in the optical property calculations for the HfO_2, SiO_2, and $HfSiO_4$ mediums. The oscillator strengths $f_{nn'}$ representing the optical transition probabilities and the relaxation coefficients $\gamma_{nn'}$ representing the optical transition relaxation process were assumed to be 0.017 and 0.05 eV for all pairs of MOs, n and n', respectively.

Medium	Number of clusters per unit volume N_m(m^{-3})	Oscillator strength $f_{nn'}$	Relaxation coefficient $\gamma_{nn'}$(eV)	Integral limits min–max(eV)
HfO_2	1.027×10^{28}	0.017	0.05	−20–30
SiO_2	4.266×10^{27}	0.017	0.05	−20–30
$HfSiO_4$	6.027×10^{27}	0.017	0.05	−20–30

Downloaded 21 Jul 2008 to 152.78.61.227. Redistribution subject to AIP license or copyright; see http://jap.aip.org/jap/copyright.jsp

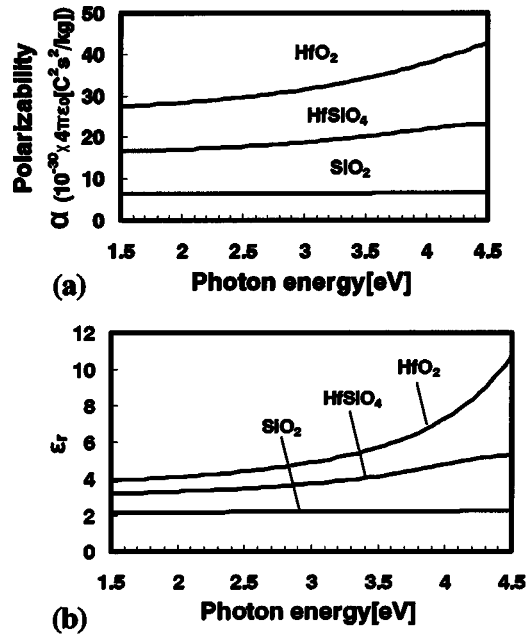

FIG. 2. The electronic optical properties of the HfO_2, SiO_2, and $HfSiO_4$ mediums. (a) The electronic polarizabilities calculated by the band-gap values and DOS distributions using Eqs. (9) and (10). (b) The electronic dielectric constants calculated from the electronic polarizabilities using Eq. (11).

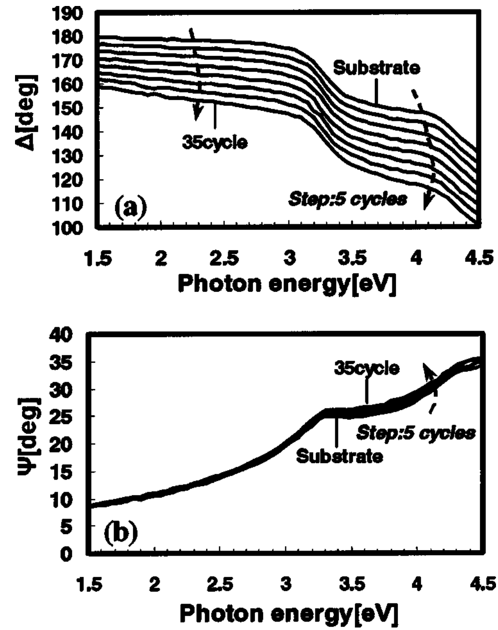

FIG. 3. Real-time spectroscopic ellipsometry spectra measured at every 5 cycles during the HfO_2 films growth. (a) The Δ decreases gradually with virtually maintaining the overall curve shape when the number of cycles increases. (b) The Ψ spectrum curve shows almost no change because it was less sensitive to the phase shift due to an increase in the film thickness.

lator strength $f_{nn'}$, which represents the optical transition probabilities between the valence and the conduction bands, and the relaxation coefficients $\gamma_{nn'}$, which represent the optical relaxation processes were assumed to be 0.017 and 0.05 eV for all pairs of MOs, n and n', respectively. The constant value of $f_{nn'}$ used for the present calculations was evaluated from the sum rule for the transition probability (i.e., the sum over all the possible transitions is unity) with the number of those MOs. We made a bit random choice for $\gamma_{nn'}$ within a reasonable energy range in order to avoid the divergence of the calculations,[18] but it was confirmed that the results are virtually independent of the choice of the value.

Figures 2(a) and 2(b) show the electronic polarizability functions, $\alpha(E)$, and the real parts of the dielectric constants, $\varepsilon_r(E)$, calculated for the three amorphous films. The values of $\varepsilon_r(E)$ calculated for SiO_2 and HfO_2 are in good agreement with the experimental values, in particular at low energies, of 2.11 for SiO_2 (Ref. 24) and that of 3.79 for HfO_2 (Ref. 25) measured at the energy of 1.5 eV. The imaginary parts of the dielectric functions, $\varepsilon_i(E)$, which are related to the light absorption, are zero for these mediums because the incident photon energies are less than the band gaps, and the optical transition probabilities are virtually zero. It can be seen from these theoretical results that the electronic permittivity of SiO_2 is the smallest while that of HfO_2 is the largest, and the electronic permittivity of $HfSiO_4$ is between those for SiO_2 and HfO_2, as guessed by intuition. The $\varepsilon_r(E)$ curve for SiO_2 is flatter than those for $HfSiO_4$ and HfO_2, which both show a monotonic increase in the high-energy region. It is mainly because their band-gap values and DOS distributions are significantly different. Actually, because the photon energies are less than the band gaps $(\omega < \omega_{nn'})$ in Eq. (11), it is apparent that the material with a smaller band gap would show a larger electronic permittivity if we have two materials with the same DOS distributions. Also, the material with the higher DOS near the band gap would show a larger electronic permittivity if we compare two materials with the same band gap. A steeper increase seen for HfO_2 in the high-energy region is supposed to result from the constant approximation used for calculating the oscillator strengths, which does not work properly in the high-energy region.

Based on the above arguments on the band gap and DOS distribution concerning the $Hf_xSi_yO_z$, one can predict that, in general, if the compositional ratio of Hf is greater than that of Si $(x > y)$, the $\varepsilon_r(E)$ curve of $Hf_xSi_yO_z$ would be closer to that of HfO_2, inversely, if the compositional ratio of Si is greater than that of Hf $(x < y)$, the $\varepsilon_r(E)$ curve of $Hf_xSi_yO_z$ would be closer to that of SiO_2.

IV. RESULTS AND DISCUSSION

Before conducting the *in situ* real-time spectroscopic ellipsometry, we measured the $C-V$ and $I-V$ characteristics for HfO_2 thin film deposited in the optimized conditions described in Sec. II. The EOT and the leakage current density at a bias voltage of −1 V were 1.61 nm and 1.75×10^{-3} A/cm^2, respectively, indicating that the films have good electrical characteristics as the high-k gate dielectrics. Figure 3 shows the real-time spectroscopic ellipsometry spectra taken at every 5 cycles during the film growth. We observed that Δ decreases gradually with virtually maintaining the overall curve shape when the number of cycles increases. On the other hand, the Ψ spectrum curve shows little change because it was less sensitive to the phase shift caused by an increase in the film thickness.

By using Δ and Ψ measured before the film deposition (i.e., only the Si substrate) and then after every 5 cycles of

Downloaded 21 Jul 2008 to 152.78.61.227. Redistribution subject to AIP license or copyright; see http://jap.aip.org/jap/copyright.jsp

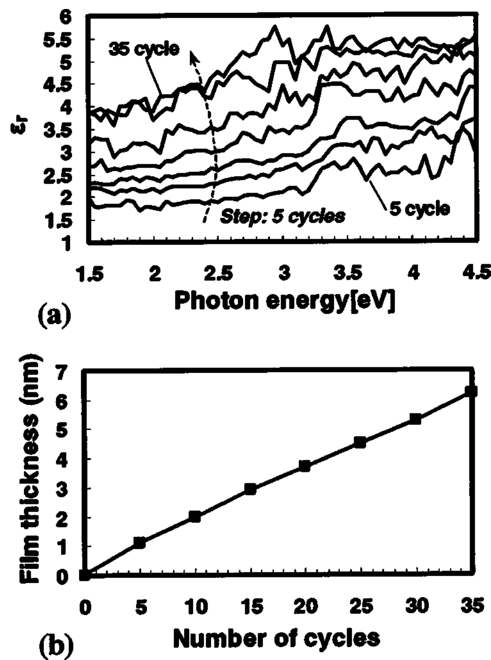

FIG. 4. (a) Photon energy dependence of average dielectric constants measured at every 5 cycles and (b) the total film thickness as a function of the number of cycles.

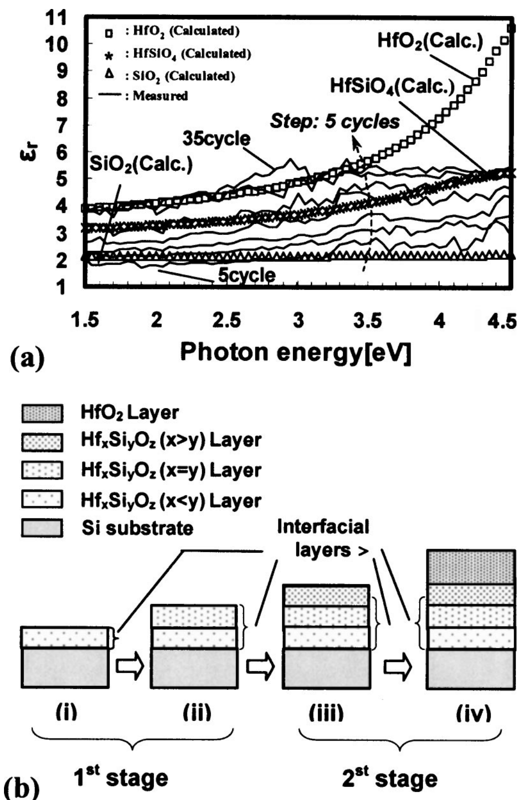

FIG. 5. (a) Comparison of the experimental results obtained from SE spectra with the theoretical results for HfO_2, SiO_2, and $HfSiO_4$. (b) A schematic diagram of two different growth processes: the first stage in which formation of the interfacial layers is dominant and the second stage in which formation of pure hafnia is dominant.

the deposition, the dielectric constant ε_r (real part of ε) averaged over the entire film and the film thickness were evaluated as described in Sec. II. Figure 4 shows the photon energy dependence $\varepsilon_r(E)$ [Fig. 4(a)] and the change in the film thickness as a function of the number of cycles [Fig. 4(b)], respectively. In Fig. 4(a), the ε_r curves lie in the range from 2 to 6 during the film growth, and the average dielectric constant of the film gradually increases when the number of cycles increases. On the other hand, the film thickness increases almost linearly as shown in Fig. 4(b), indicating that the growth rate was constant during the deposition. The film thickness after 5 and 35 cycles were 2.0 and 6.2 nm, respectively.

Figure 5(a) compares these experimental results obtained from the SE spectra with the theoretical results shown in Sec. III. It can be seen that the value of ε_r obtained for less than 5 cycles is close to the calculated results for the SiO_2. With the increase in the number of cycles, overall ε_r increases gradually and appears to settle in its steady position finally. In particular, ε_r obtained after 35 cycles ranges from 4 to 6, which is relatively close to the calculated dielectric constants of the HfO_2. It should also be noted that the average dielectric constants for the film before the 15 cycles are between two theoretical dispersion curves for SiO_2 and $HfSiO_4$, and with the increase of the number of cycles, the dielectric constant curves of the film approache to that for $HfSiO_4$ gradually. This indicates the formation of $Hf_xSi_yO_z$ layers during which the composition ratio of Hf to Si (x/y) varies from almost 0 to 1 with the increase in the number of cycles. After the 15 cycles, the average dielectric constants of the film are between the theoretical curves for $HfSiO_4$ and HfO_2. The dielectric constant curves finally reach the steady position near that of HfO_2, indicating that HfO_2 layer formation is eventually dominant. This trend is clear for the photon energy up to 3.5 eV, but the difference between the theoretical and experimental results is apparent above 3.5 eV. This is attributed to the energy-independent oscillator strength approximation adopted in our calculations mentioned in Sec. III.

These results indicate that the HfO_2 film growth process can be divided into two stages [see Fig. 5(b)], which have different growth mechanisms, the first stage ($\sim$15 cycles) in which formation of the interfacial layers consisting of $Hf_xSi_yO_z$ is dominant, and the second stage (15 cycles$\sim$) in which formation of pure HfO_2 is dominant. Figures 6 and 7 illustrate the cross-section TEM image and the composition analysis by EDX for the HfO_2 thin films under investigation. In the TEM images shown in Fig. 6, we confirmed that the total thickness of the film and that of the interfacial layer were approximately 6.9 and 2.1 nm, respectively, which are in good agreement with 2.0 and 6.2 nm estimated from the SE spectra. Furthermore, we found from the element distribution profiles across the film obtained by using EDX analysis that the concentrations of Hf and O increase in the interfacial layer region while the concentration of Si decreases gradually in the direction from the substrate to the surface $(\langle 1 \rangle \rightarrow \langle 2 \rangle)$. Above the interfacial layer the concentrations of Hf and O are relatively high while the concentration of Si is virtually zero. The interfacial layer is supposed to be a $Hf_xSi_yO_z$ layer in which the ratio of Hf to Si (x/y) increased gradually, and the upper layer is mainly composed of HfO_2.

Downloaded 21 Jul 2008 to 152.78.61.227. Redistribution subject to AIP license or copyright; see http://jap.aip.org/jap/copyright.jsp

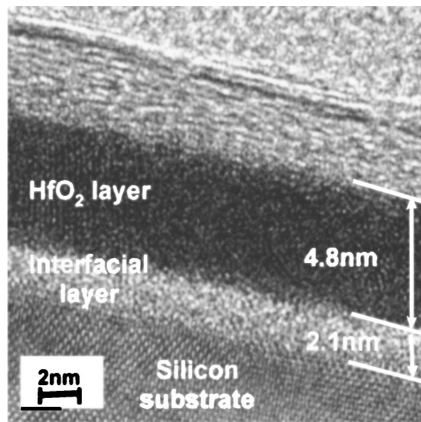

FIG. 6. TEM image of the HfO_2 thin film deposited by pulsed-source MOCVD in the optimized conditions described in Sec. II. The thickness of interfacial layer and total film were approximately 2.1 and 6.9 nm, respectively.

V. SUMMARY AND CONCLUSIONS

We investigated the growth process of the HfO_2 thin film and its dielectric properties by using the *in situ* real-time spectroscopic ellipsometry combined with the first-principles MO calculations. Particular attention was paid to the formation of the interfacial layer at an early stage of the growth process. The results obtained from this study are summarized as follows:

(1) The real-time spectroscopic ellipsometry spectra were measured every 5 cycles during the growth process, and the energy-dependent average dielectric constants were evaluated as a function of the number of cycles. With increasing the number of cycles, we observed that the dielectric dispersion curves move gradually from that for SiO_2 to that for HfO_2.

(2) The DOS distributions were calculated for the HfO_2, SiO_2, and $HfSiO_4$ clusters by using the DV-$X\alpha$ first-principles MO method. The obtained band gaps were 4.9, 10.5, and 4.6 eV for HfO_2, SiO_2, and $HfSiO_4$, respectively. The results show that the occupied MOs consist mainly of the O-2*s* and O-2*p* orbitals while the unoccupied MOs consist of the Hf-5*d*, Hf-6*s*, and Hf-6*p* orbitals for HfO_2 and the Si-3*p*, Si-3*d*, and Si-3*s* orbitals for SiO_2. Based on the calculated electronic states, the electronic polarizabilities and dielectric functions for these three clusters were then computed. We found that the dielectric function for SiO_2 is the smallest while that of HfO_2 is the largest, and the dielectric function of $HfSiO_4$ is between them. The electronic states and the dielectric functions for the intermediate $Hf_xSi_yO_z$ structures can also be estimated approximately from these results.

(3) The experimental and theoretical results in (1) and (2) were compared to analyze the gradual change in the dielectric constants during the HfO_2 film growth. We found that the HfO_2 film growth process can be divided into two stages which have different growth mechanisms: the first stage ($\sim$15 cycles) with the growth of SiO_2 or $Hf_xSi_yO_z$ layers and the second stage (15 cycles$\sim$) with the formation of HfO_2 layers predominantly. SiO_2 and $Hf_xSi_yO_z$ layers grown during the first stage can be regarded as the interfacial layers. All these results look consistent with the film structure analysis by using TEM and the film composition analysis by using EDX.

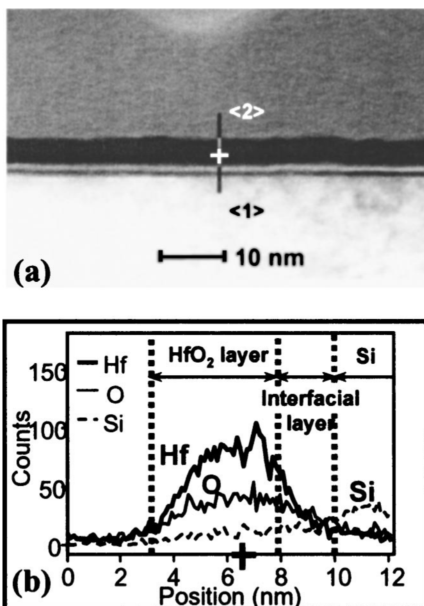

FIG. 7. Composition analysis for the HfO_2 thin film deposited by pulsed-source MOCVD in the optimized conditions described in Sec. II by EDX evaluation. (a) Scanning TEM dark field image of the sample. The solid line was the location for line scan of EDX analysis. (b) The distribution profile of the Hf, O, and Si along the solid line in (a).

ACKNOWLEDGMENTS

The authors would like to acknowledge IME Singapore Inc. with the cross-sectional TEM images and EDX analysis for the HfO_2 thin-film samples. The authors also gratefully acknowledge Dr. M. Okamoto, Mechanical Research Laboratory, Hitachi Ltd., for providing useful information about the first-principles calculations on SiO_2 and HfO_2. One of the authors (Y.D.Z) thanks ShaoYun Huang in the same laboratory for helpful discussions.

APPENDIX: DV-$X\alpha$ CALCULATIONS FOR THE HfO_2, SiO_2, AND $HfSiO_4$ CLUSTERS

The electronic states of the amorphous films can be approximately described by that of the unit clusters extracted from the amorphous random-network structures. We chose a first-principles molecular-orbital (MO) calculation, the nonrelativistic discrete-variational $X\alpha$ (DV-$X\alpha$) method developed by Ellis and Painter,[26] Ellis and Rosen,[27] and Adachi *et al.*[28] to calculate the electronic states of the clusters, using a program code SCAT.[28] This method bases on the Hartree–Fock–Slater equations shown in Eq. (A1), and the exchange and correlation energies are taken into account by the use of $X\alpha$ potential given by Eq. (A2).[29]

Downloaded 21 Jul 2008 to 152.78.61.227. Redistribution subject to AIP license or copyright; see http://jap.aip.org/jap/copyright.jsp

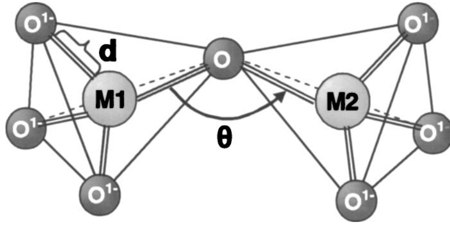

FIG. 8. Cluster models extracted from random network of the amorphous thin film for DV-Xα calculations. The large circles are for Si or Hf and the small circles are for O or O^{-1}. The sticks are for the bonds. In the case of SiO_2 cluster, both of the $M1$ and $M2$ are Si atoms, Si–O bond length $d=1.62$ Å (Ref. 35) and Si–O–Si bond angle $\theta=135°$ (Refs. 36 and 37). In the case of HfO_2 cluster, both of the $M1$ and $M2$ are Hf atoms, Hf–O bond length $d=2.10$ Å (Ref. 38) and Hf–O–Hf bond angle $\theta=135°$. In the case of $HfSiO_4$ cluster, $M1$ is a Si atom and $M2$ is a Hf atom, Si–O bond length $d1=1.62$ Å and Hf–O bond length $d2=2.10$ Å, Si–O–Hf bond angle $\theta=135°$.

$$\left[-\frac{1}{2}\nabla_1^2-\sum_v \frac{Z_v}{r_{1v}}+\int \frac{\rho(\boldsymbol{r}_2)}{r_{12}}d\boldsymbol{r}_2+V_{XC\uparrow}(\boldsymbol{r}_1)\right]\Phi_{k\uparrow}(\boldsymbol{r}_1)=\varepsilon_{k\uparrow}\Phi_{k\uparrow}(\boldsymbol{r}_1), \tag{A1}$$

$$V_{XC\uparrow}(\boldsymbol{r}_1)=-3\alpha\left\{\frac{3}{4\pi}\rho_\uparrow(\boldsymbol{r}_1)^{1/3}\right\}, \tag{A2}$$

where $\varepsilon_{k\uparrow}$ is the MO energy and $\rho_\uparrow(\boldsymbol{r}_1)$ is the local charge density calculated by Eq. (A3),

$$\rho_\uparrow(\boldsymbol{r}_1)=\sum_{k\uparrow} f_{k\uparrow}\Phi_{k\uparrow}(\boldsymbol{r}_1)\Phi_{k\uparrow}(\boldsymbol{r}_1). \tag{A3}$$

The parameter α is fixed at a constant of 0.7 suitable for transitional metal compounds.[30,31] MOs are constructed by linear combination of atomic orbitals (LCAO) as follows:

$$\Phi_k(\boldsymbol{r}_1)=\sum_j c_{jk}\chi_j(\boldsymbol{r}_1), \tag{A4}$$

where $\chi_i(\boldsymbol{r}_1)$ denotes the AO as a numerical basis function solved from the Schrödinger's equations of the atoms, and the coefficients c_{jk} are corresponding to the density of states (DOS). Self-consistent charge calculation with degree of convergence within 0.01% of the Muulliken charge was made to accomplish the self-consistent-field calculation practically.[32]

The electronic states of the HfO_2, SiO_2, and $HfSiO_4$ clusters which were used to approximate the amorphous mediums formed in the HfO_2 film growth were calculated in this study. The structure of amorphous SiO_2 glass is best described by the continuous random-network model in which the Si atom is tetrahedrally bonded to four O atoms and the O atom bridges between two Si atoms with a very flexible Si–O–Si bridging angle.[33–35] As a qualitative analysis, the amorphous HfO_2 and $HfSiO_4$ were assumed to have the same structure as the amorphous SiO_2. Figure 8 shows the unit cluster model extracted from the amorphous random network. The O atoms having only one bond to metal atoms were replaced by the ion O^{-1} for charge balance. The values of bond length and bond angle for the three clusters were referred to the experimental or theoretical values in the literatures.[36–38]

TABLE II. Positions of atoms or ions in the HfO_2, SiO_2, and $HfSiO_4$ clusters.

Cluster	Atom or ion	x(Å)	y(Å)	z(Å)
	Hf-1	−1.918	0.000	−0.855
	Hf-2	1.918	0.000	−0.855
	O	0.000	0.000	0.000
	O^{1-}-1	−3.363	0.000	0.669
HfO_2	O^{1-}-2	3.363	0.000	0.669
	O^{1-}-3	−2.155	−1.715	−2.044
	O^{1-}-4	2.155	−1.715	−2.044
	O^{1-}-5	−2.155	1.715	−2.044
	O^{1-}-6	2.155	1.715	−2.044
	Si-1	−1.480	0.000	−0.659
	Si-2	1.480	0.000	−0.659
	O	0.000	0.000	0.000
	O^{1-}-1	−2.595	0.000	0.516
SiO_2	O^{1-}-2	2.595	0.000	0.516
	O^{1-}-3	−1.662	−1.323	−1.577
	O^{1-}-4	1.662	−1.323	−1.577
	O^{1-}-5	−1.662	1.323	−1.577
	O^{1-}-6	1.662	1.323	−1.577
	Si	−1.480	0.000	−0.659
	Hf	1.918	0.000	−0.855
	O	0.000	0.000	0.000
	O^{1-}-1	−2.595	0.000	0.516
$HfSiO_4$	O^{1-}-2	3.363	0.000	0.669
	O^{1-}-3	−1.662	−1.323	−1.577
	O^{1-}-4	2.155	−1.715	−2.044
	O^{1-}-5	−1.662	1.323	−1.577
	O^{1-}-6	2.155	1.715	−2.044

According to the cluster model in Fig. 8, we calculated the coordinate values of the atoms or ions in the clusters shown in Table II. All the calculations of the energy levels and DOS were performed using these data. In our calculations, we used the basis functions of $1s-6d$ for Hf atoms, $1s-3d$ for Si atoms, and $1s-2p$ for O atoms. To describe the occupied MO and unoccupied MO states, the outermost orbitals involved in the calculations were chosen to be $(5d,6s,6p)$ for Hf atoms, $(3s,3p,3d)$ for Si atoms, and $(2s,2p)$ for O atoms. The DOS profile is given by replacing each discrete level by a Lorentzian with a width of 0.05 eV, weighted by the degeneracy of the orbitals, so that DOS of the occupied MOs and unoccupied MOs near the band gap can be considered to represent that of the valence bands and the conduction bands of the film.

[1] *The International Technology Roadmap for Semiconductors, 2002* (Semiconductor Industry Association, San Jose, CA, 2002).
[2] G. D. Wilk, R. M. Wallace, and J. M. Anthony, J. Appl. Phys. **89**, 5243 (2001), and references therein.
[3] K. J. Hubbard and D. G. Schlom, J. Mater. Res. **11**, 2757 (1996), and references therein.
[4] L. F. Schneemeyer, R. B. van Dover, and R. M. Fleming, Appl. Phys. Lett. **75**, 1967 (1999).
[5] S. J. Lee, H. F. Luan, W. P. Bai, C. H. Lee, T. S. Jeon, Y. Senzaki, D. Roberts, and D. L. Kwong, Tech. Dig. - Int. Electron Devices Meet. **2000**, 31.
[6] L. Kang *et al.*, Tech. Dig. - Int. Electron Devices Meet. **2000**, 35.
[7] B. H. Lee *et al.*, Tech. Dig. - Int. Electron Devices Meet. **2000**, 39.
[8] B. K. Park, J. Park, M. Cho, C. S. Hwang, K. Oh, Y. Han, and D. Y. Yang, Appl. Phys. Lett. **80**, 2368 (2002).

Downloaded 21 Jul 2008 to 152.78.61.227. Redistribution subject to AIP license or copyright; see http://jap.aip.org/jap/copyright.jsp

[9]Y. Tsuchiya, M. Endo, M. Kurosawa, R. T. Tung, T. Hattori, and S. Oda, Jpn. J. Appl. Phys., Part 1 **42**, 1957 (2003).
[10]http: //global.horiba.com/optics/products/elli/uvisel/
[11]R. W. Collins, Appl. Phys. Lett. **48**, 843 (1986).
[12]S. Kumar, B. Drevillon, and C. Godet, J. Appl. Phys. **60**, 1542 (1986).
[13]N. Layadi, P. Rocai Cabarrocas, J. Huc, J. Y. Parey, and B. Previllon, Solid State Phenom. **37/38**, 281 (1994).
[14]B. Drevillon, J. Y. Parey, M. Stchakovsky, R. Benferhat, Y. Josser, and B. Schlayen, Proc. SPIE **1188**, 174 (1990).
[15]R. M. A. Azzam and N. M. Bashara, *Ellipsometry and Polarized Light* (North-Holland, Amsterdam, 1977).
[16]M. Born and E. Wolf, *Principles of Optics* (Pergamon, Oxford, 1965).
[17]J. J. Sakurai, *Advanced Quantum Mechanics* (Addison-Wesley, Reading, MA, 1967).
[18]W. Heitler, *The Quantum Theory of Radiation*, 3rd ed. (Dover, New York, 1984).
[19]J. Robertson, MRS Bull. **27**, 217 (2002).
[20]Y.-N. Xu and W. Y. Ching, Phys. Rev. B **44**, 11048 (1991).
[21]N. Binggeli, N. Troullier, J. L. Martins, and J. R. Chelikowsky, Phys. Rev. B **44**, 4771 (1991).
[22]J. Kang, E.-C. Lee, and K. J. Chang, Phys. Rev. B **68**, 054106 (2003).
[23]A. S. Foster, F. L. Gejo, A. L. Shluger, and R. M. Nieminen, Phys. Rev. B **65**, 174117 (2002).
[24]E. D. Palik, *Handbook of Optical Constants of Solids* (Academic, New York, 1985).
[25]J. P. Borgogno, B. Lazarides, and E. Pelletier, Appl. Opt. **21**, 4020 (1982).
[26]D. E. Ellis and G. S. Painter, Phys. Rev. B 2, 2887 (1970).
[27]D. E. Ellis and A. Rosen, Z. Phys. A **283**, 5 (1977).
[28]H. Adachi, M. Tsukada, and C. Satoko, J. Phys. Soc. Jpn. **45**, 875 (1978).
[29]J. C. Slater, *Quantum Theory of Molecules and Solids* (McGraw-Hill, New York, 1974), Vol. 1–4.
[30]E. J. Baerends and P. Ross, Chem. Phys. **2**, 52 (1973).
[31]K. Schwarz, Phys. Rev. B **5**, 2466 (1972).
[32]H. Adachi, A. Rose'n, and D. E. Ellis, Mol. Phys. **33**, 199 (1977).
[33]F. L. Galeener, in *The Physics and Technology of Amorphous* SiO_2, edited by R. A. B. Devine (Plenum, New York, 1987), p. 1.
[34]W. H. Zachariasen, J. Am. Chem. Soc. **54**, 3841 (1932).
[35]B. E. Warren, J. Appl. Phys. **8**, 645 (1937).
[36]A. H. Edwards, Phys. Rev. Lett. **71**, 3190 (1993).
[37]K. Hirose, H. Kitahara, and T. Hattori, Phys. Rev. B **67**, 195313 (2003).
[38]X. Y. Zhao and D. Vanderbilt, Phys. Rev. B **65**, 233106 (2002).

Downloaded 21 Jul 2008 to 152.78.61.227. Redistribution subject to AIP license or copyright; see http://jap.aip.org/jap/copyright.jsp